Volume 8
Number 41
7 November 2020
Pages 9377–9612

Journal of Materials Chemistry B

Materials for biology and medicine

rsc.li/materials-b

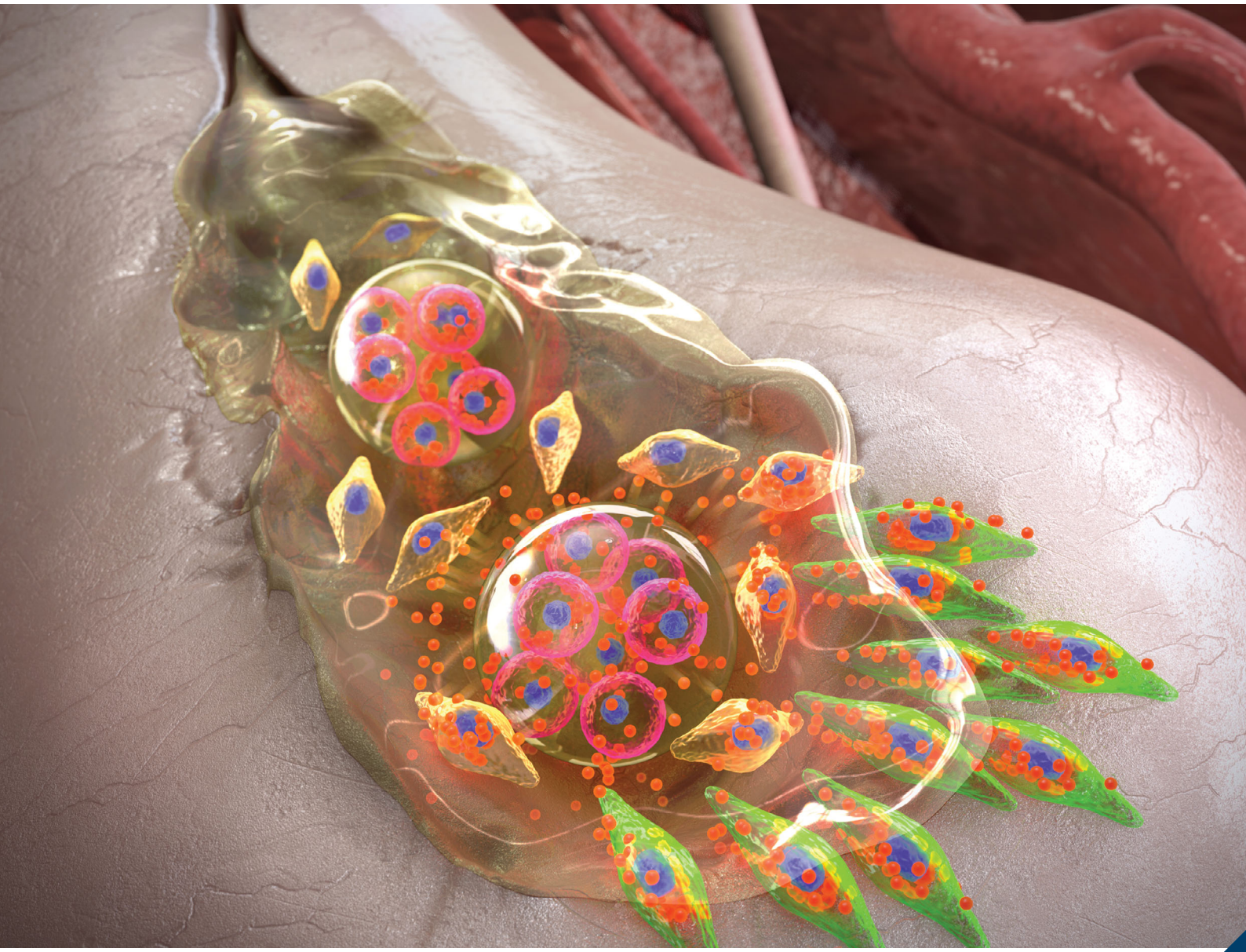

ISSN 2050-750X

ROYAL SOCIETY OF CHEMISTRY

PAPER

Won-Gun Koh, Jae Hyup Lee, Kangwon Lee *et al.*
A novel 3D indirect co-culture system based on a collagen hydrogel scaffold for enhancing the osteogenesis of stem cells

Indexed in Medline!

Journal of Materials Chemistry B

ROYAL SOCIETY OF CHEMISTRY

PAPER

Cite this: J. Mater. Chem. B, 2020, 8, 9481

A novel 3D indirect co-culture system based on a collagen hydrogel scaffold for enhancing the osteogenesis of stem cells

Hyerim Kim,†[a] Shi Huan Han,†[bc] Yun-Min Kook,†[d] Kyung-Mee Lee,[e] Yuan-Zhe Jin,[f] Won-Gun Koh,*[g] Jae Hyup Lee*[beh] and Kangwon Lee*[a]

Received 20th July 2020,
Accepted 11th September 2020

DOI: 10.1039/d0tb01770a

rsc.li/materials-b

In this study, the paracrine effect between adipose-derived mesenchymal stem cells (ADSCs) and osteoblasts was investigated in collagen-based three-dimensional (3D) scaffolds. 3D encapsulation of mesenchymal stem cells in hydrogel scaffolds was conducted for bone tissue regeneration. Osteoblasts were encapsulated in alginate microbeads with uniform size, which could be controlled by varying the supply voltage using electrostatic droplet extrusion. Osteoblast-encapsulated microbeads were embedded with ADSCs in collagen bulk hydrogel scaffolds with a high survival rate. The separated space between the two types of cells made it possible to confirm ADSC differentiation into osteogenic lineages in the 3D collagen hydrogel scaffold by the paracrine effect *in vitro*. Furthermore, co-cultured ADSC and osteoblasts showed enhanced bone formation compared with the ADSC monoculture group in the rat calvarial defect model. The system developed in this study provides a novel *in vitro* tissue model for bone regeneration without exogenous factors, and it has the potential to be used to study the paracrine effect in various co-culture systems in the near future.

1. Introduction

Bone is essential to all human beings to maintain posture and protect other organs, neurons, and the brain. Bone defects and structural loss caused by trauma and several diseases, such as osteoporosis, osteomalacia, and osteodystrophy, entail tremendous disruption of a healthy life.[1,2] Despite the high incidence and difficult treatment of bone malfunction, few clinically available treatments are simple and have a low patient burden.

Therapeutic clinical strategies for open reduction usually fix a bone fracture with special screws or metal plates applied to the outer surface of the bone. These surgical operations help to rectify bone fractures; however, additional support should be considered to accelerate bone repair and remodeling. Moreover, autogenous bone transplantation has been considered to be optimal for successful bone grafting.[3–5] However, despite tissue compatibility, these approaches have the limitations of donor site morbidity, lack of sources, and prolonged healing time.[6–8]

To overcome the low regeneration capacity of conventional clinical trials for successful bone regeneration, therapeutic strategies of cell-based therapy using stem cells alone[9–12] or in combination with osteogenic cells[13] have been used to reconstitute or regenerate damaged bone. For successful bone regeneration, a multicellular microenvironment that consists of stem cells, osteoblasts, and other types of cells is necessary. In natural bone, several types of cells, including osteoblasts, osteocytes, and stem cells, interact with each other through direct cell–cell contact and soluble factors.[14–16] In addition, physiological support using a scaffold is needed to mimic a natural three-dimensional (3D) environment and enhance cell viability after implantation into the defect site.[4] To mimic a multicellular microenvironment of bone tissue and accelerate osteogenic differentiation of stem cells, various co-culture systems have been developed. For example, a mix of stem cells

[a] Program in Nanoscience and Technology, Graduate School of Convergence Science and Technology, Seoul National University, Seoul, Korea. E-mail: kangwonlee@snu.ac.kr
[b] Department of Orthopedic Surgery, College of Medicine, Seoul National University, Seoul, 03080, Korea. E-mail: spinelee@snu.ac.kr
[c] Department of Orthopedic Surgery, YanBian University Hospital, 133000, Yanji, Jilin Province, China
[d] Center for Biomaterials, Biomedical Research Institute, Korea Institute of Science and Technology (KIST), Seoul, Korea
[e] Department of Orthopedic Surgery, SMG-SNU Boramae Medical Center, Seoul, 07061, Korea
[f] Department of Spine Surgery, The First Hospital of Jilin University, 130021, Changchun, Jilin Province, China
[g] Department of Chemical and Biomolecular Engineering, Yonsei University, Seoul, Korea. E-mail: wongun@yonsei.ac.kr
[h] Institute of Medical and Biological Engineering, Seoul National University, Seoul, 110-799, Korea
† Contributed equally.

and osteoblasts in the monolayer culture as a direct co-culture was studied for studying cell–cell interaction effects and osteogenic capacity.[17,18] Also, a trans-well co-culture system was performed for delicate investigation of crosstalk between stem cells and osteoblasts.[18,19] Although several studies have found that a co-culture system of stem and osteogenic cells is effective for stem cell differentiation, most of them used a two-dimensional (2D) monolayer culture.[20,21] Although the 3D co-culture model of stem cells is known to be a good candidate for a therapeutic approach, continuous cytokine or growth factor delivery to stem cells is not contained. This is the essential biological and chemotactic effect observed in the stem cell differentiation mechanism. Moreover, stem cell differentiation in a single co-culture batch should be investigated for further pathological study of stem cell therapy.

Given the importance of the delivery of growth factors or cytokines for stem cell differentiation, sustained delivery using microgels has been developed as a cargo to encapsulate cells and bioactive molecules. Because microgels exhibit several benefits in drug delivery and transplantation systems, various studies on encapsulating cells and soluble factors in microgels have been reported. Several simple procedures to synthesize microgels produce highly tunable and monodispersed microspheres.[22] Besides, microgels can protect encapsulated cells and drugs from harmful side effects from unexpected delivery[23] and cells in microgels could enhance the paracrine effect. For example, drugs in biocompatible chitosan–gelatin based microgels sustainedly released within several days[24] and mesenchymal stem cells (MSCs) in collagen-based microgels exhibited enhanced angiogenic cytokine expression which enabled hindlimb ischemia regeneration.[25] Thus, based on the sustained and stable delivery behavior of microgels could be an insightful candidate for tissue regeneration application.

In this study, a novel 3D indirect co-culture system based on collagen hydrogel containing alginate microbeads with osteoblasts was fabricated. An attempt was made to explore the efficacy of this 3D co-culture system for cell proliferation viability, as well as stem cell differentiation into osteogenic cell lines. A comparison with the conventional growth factor effect on bone regeneration based on stem cells in the calvarial defect model was made. Stem cells cultured in 3D collagen hydrogels with osteoblast containing alginate microbeads exhibited osteogenic differentiation with increased osteogenic functions. This result suggests that this new 3D indirect co-culture system can enable bone formation that is more robust and functionally possible.

2. Experimental

2.1 Preparation of alginate microbeads and 3D collagen hydrogel scaffolds

Alginate microbeads were fabricated by electrostatic droplet extrusion (NanoNC, #ESR100D). Alginate (Wako, Japan) was dissolved in deionized water to form a 2 wt% solution. Then, a 9 kV electrical potential was applied to the syringe pump containing alginate solution through a 27-gauge stainless-steel needle with a continuous 5 mL h^{-1} flow rate. The alginate solution was dropped from the needle and collected in a 75 mM calcium chloride (Sigma Aldrich, USA) solution at the bottom of an extrusion machine. The collected alginate microbeads were washed with phosphate-buffered saline (PBS). For cell study, alginate microbeads were mixed with a 5 wt% collagen solution (Corning, #354249) in an ice bath, and the mixture was transferred to a customized 8 mm-diameter mold and then neutralized with 1 N NaOH. The collagen solution was incubated at 37 °C for 30 min for gelation.

2.2 Characterization of alginate microbeads and scaffolds

The collected alginate microbeads with different electrical potentials were observed using optical microscopy, and the diameters were calculated with ImageJ.

The mechanical properties of only the collagen scaffold and the collagen scaffold containing alginate microbeads were determined using Instron 5900 (Instron Corporation, USA). The scaffolds were compressed to 20% the height of the scaffolds. The stress–strain curve was obtained by measured compressive stress and compressive strain, and Young's modulus was calculated with the slope of the linear area in the curve.

2.3 Cell culture

Human adipose-derived stem cells (ADSCs) were purchased from Cefobio (#CB-ADMSC-001) and cultured in Dulbecco's modified Eagle's medium (Wellgene Inc., Korea) with 1% penicillin/streptomycin and 10% fetal bovine serum (FBS; CellSera, Australia). Osteoblasts (MC3T3-E1) were purchased from ATCC (#CRL-2593) and cultured in Alpha Minimum Essential Medium (Gibco, #A1049001) containing 1% penicillin/streptomycin and 10% FBS. Cells were incubated at 37 °C in a humid atmosphere with 5% CO_2. The growth medium was changed every two days.

2.4 Fabrication of indirect co-culture scaffolds

To develop a co-culture system in a collagen scaffold, osteoblast-encapsulating alginate microbeads (OB-beads) were fabricated using an electrostatic droplet extrusion method. First, 0.5 mL of osteoblast suspension (5×10^6 cells per mL) was mixed into 1.5 mL of 2 wt% alginate solution and then dropped with 9 kV electrical potential. Then, alginate microbeads containing osteoblasts were collected for 8 seconds, and 20 μL of ADSC suspension (2×10^6 cells per mL) were embedded in collagen solution with OB-beads to encapsulate in a single scaffold. This was followed by neutralization and gelation at 37 °C for the co-cultured collagen scaffold (AD + OB-beads). This was followed by neutralization and gelation at 37 °C for the co-cultured collagen scaffold (AD + OB-beads). The indirect co-culture system in AD + OB-beads was confirmed by staining ADSCs with green and OB with red fluorescence CellTracker staining for 30 min at 37 °C before cell encapsulation. The stained cells in the collagen scaffold were observed with a laser scanning microscope (Carl Zeiss, Germany).

For the bone morphogenetic protein-2 (BMP-2) effect on ADSCs, BMP-2-encapsulated microbeads (BMP2-beads) embedded with ADSCs in a collagen scaffold (AD + BMP2-beads) were treated as the positive control group (AD + BMP2-beads) in all cell studies. BMP-2 (R&D Systems, #GF166) (5 μg mL^{-1}) was encapsulated in alginate microbeads using the same electrostatic droplet extrusion process. Briefly, a solution mixed with 0.5 mL of BMP-2 suspension (5 μg mL^{-1}) and 1 mL of 2 wt% alginate solution was used, and BMP-2 encapsulated microbeads were collected for 9 seconds to be encapsulated in a single scaffold. ADSCs were embedded with bare alginate microbeads in a collagen scaffold and used as the negative control group (AD).

2.5 Cell viability assay

To assay the cell viability, the LIVE/DEAD Viability/Cytotoxicity Kit (Invitrogen, #L3224) was used according to the manufacturer's protocol. Cells embedded in scaffolds were immersed in the growth media with 4 mM calcein AM (green) and 2 mM ethidium homodimer-1 (red) and incubated for 30 min at room temperature. After completion of staining, the scaffolds were washed three times with PBS. The stained cells were visualized with a laser scanning microscope.

2.6 Cell proliferation assay

ADSC and osteoblast proliferation in the scaffold was assessed with the Cell Counting Kit-8 assay (CCK-8, Dojindo, #CK04-13). Cell-embedded scaffolds were washed with PBS and immersed in free media with 10% CCK-8 solution for 3 h at 37 °C. After incubation, the supernatant was collected on a 96 well plate and measured at 450 nm absorbance using a microplate reader (Biotek, USA).

2.7 BMP-2 ELISA assay

The BMP-2 release behavior by BMP2-beads and OB-beads was detected using the BMP-2 ELISA kit (R&D Systems, #E-EL-H0011). BMP2-beads were incubated in 2 mL PBS and collected at different time points (days 1, 4, 7, 14, 21, and 28). Osteoblast-encapsulated alginate microbeads were incubated in 2 mL of growth media and collected at the same time points as BMP2-beads. The concentration of the collected solution was measured using the ELISA kit according to the manufacturer's protocol.

2.8 ALP activity

The alkaline phosphatase (ALP) activity of each scaffold (n = 3 per group) was measured with a LabAssay ALP kit (Wako Pure Chemicals, #291-58601). The scaffolds of positive and negative groups were incubated in a lysis buffer for 30 min at 37 °C. The indirect co-culture scaffolds were treated with collagenase type I (Millipore #SCR103) for 30 min at 37 °C to remove the OB-beads. The collected ADSCs were incubated in the lysis buffer. The supernatant was collected to observe ALP activity according to the manufacturer's instructions. The ALP activity level was normalized using a BCA protein assay kit (Thermo Fisher, #23227).

2.9 Immunofluorescence staining

Immunofluorescence staining of osteogenesis markers (ALP, collagen type I, osteocalcin (OCN)) was conducted with an OCT compound block containing scaffolds. The scaffolds were fixed with 4% paraformaldehyde for 30 min at room temperature and washed with PBS. The scaffolds were dehydrated in 30% sucrose solution overnight at 4 °C. The treated scaffolds were rinsed with PBS, embedded in the OCT compound, and sequentially immersed in liquid nitrogen. The frozen scaffolds were sectioned at 6 cm thickness. The sectioned scaffolds were blocked with 3% bovine serum albumin (BSA) for 1 h and permeabilized with 0.1% Triton X-100 in PBS for 15 min at room temperature. Sequentially, the primary antibodies of ALP (abcam, #ab126820), collagen type I (Millipore, #MAB3391), and OCN (abcam, #ab13421) in 1% BSA were treated and incubated overnight at 4 °C. The sections were washed with PBS three times and then treated with the second antibody goat anti-mouse IgG (abcam, #ab175473) for 1 h at room temperature. After the incubation, PBS washing and DAPI staining were performed for 10 min. The immunostained section was observed by optical microscopy.

2.10 Alizarin red S staining and quantification

The cryo-sectioned scaffolds were washed with PBS before fixation with 4% paraformaldehyde for 30 min at room temperature. Then, the samples were treated with 2% Alizarin red S solution in distilled water (pH 4.1–4.3) for 10 min at room temperature and washed with PBS three times.

For quantification of Alizarin red S solution obtained in the scaffold, all scaffolds were fixed with 4% paraformaldehyde and immersed in 2% Alizarin red S solution for 15 min. Samples were washed three times with PBS and incubated in PBS for 48 h to remove unspecific binding solution. After washing, the samples were added to 10% acetic acid and incubated at room temperature for 30 min with shaking. The acetic acid solution including the sample was heated at 85 °C for 10 min and then transferred to an ice bath for 5 min. The solution was neutralized with 10% ammonium hydroxide, and absorbance at 570 nm was measured.

2.11 Quantitative real-time polymerase chain reaction (real-time PCR)

The gene expression of osteogenesis markers, including ALP, Runx2, and OCN, was analyzed by real-time PCR assay. mRNA was isolated using TRIzol (Life Technologies) and synthesized to cDNA using a Maxime RT PreMix Kit (iNtRON Biotechnology, Korea) according to the manufacturer's instructions. Gene-level expression was performed with a Maxime PCR PreMix kit (iNtRON Biotechnology) and analyzed with an Applied Biosystems QuantStudio 5 Real-Time PCR Instrument (Thermo Fisher Scientific, United States). The sequences of primers were Actin (forward 5′-CACCATTGGCAATGAGCGGTTC-3′, reverse 5′-AGGTCTTTGCGGATGTCCACGT-3′), Runx2 (forward 5′-ATTTCTCACCTCCTCAGCCC-3′, reverse 5′-CAACAGCCACAAGTTAGCGA-3′), ALP (forward 5′-ACCATTCCCACGTCTTCACATTT-3′,

reverse 5′-AGACATTCTCTCGTTCACCGCC-3′), and OCN (forward 5′-CAAAGGTGCAGCCTTTGTGTC, reverse 5′-TCACAGTCCGGATTGAGCTCA-3′). The expressed gene levels were normalized to Actin as the house-keeping gene, and the relative gene level was calculated by the $2^{-\Delta\Delta CT}$ method.

2.12 *In vivo* study

The animal research was approved by the International Animal Care and Use Committee (SMG-SNU Boramae Medical Center, IACUC No. 2018-0021). In this animal study, 24 eight-week-old male Sprague Dawley rats (240–260 g) were used after an acclimation period of seven days. All animals were provided abundant water and food and kept in a 12 : 12 dark/light cycle and a specific-pathogen-free (SPF) cage. The 24 rats were randomly divided into the following groups: (1) AD (n = 8), (2) AD + OB-beads group (n = 8), and (3) AD + BMP2-beads group (n = 8).

For anesthesia, a mixture of 20 mg kg^{-1} Zoletil (VIRBAC S.A., Carros, France) and 10 mg kg^{-1} xylazine (Bayer Korea Co., Ansan, Korea) was used for intraperitoneal injection for animals. In addition, after the anesthesia took effect, the scalp was shaved, and the surgical site was disinfected using 10% betadine solution. Then, a longitudinal incision was made on the scalp, and an 8 mm-diameter round critical defect was produced using a trephine bur. After the defect site was washed with the saline solution, the scaffold was implanted into the defect site, and the scalp was carefully sutured with a 4-0 nylon thread. To prevent infection, 100 mg kg^{-1} of Cefazolin (Chong Kun Dang Corp., Seoul, Korea) antibiotic was injected for two days after surgery.

Under deep anesthesia, all animals were sacrificed using a CO_2 chamber on their sixth week post-operation. All the specimens were harvested and immediately fixed in 10% formalin for histological examination and micro computed tomography (micro-CT) evaluation.

2.13 *In vivo* evaluation

2.13.1 Micro-CT. The specimens that included peri-implant tissues were scanned using a SkyScan 1172 (Bruker, Belgium) CT scanner. The scanner settings were 13.38 μm image pixel size, 59 kV source energy, 0.5 mm AI filter, 167 μA source current, and the 0.45° rotation step. NRecon (Bruker, Belgium, V1.7.0.4) and micro-CT (SkyScan, Bruker, Belgium, V1.17.7.2+) were used for image reconstruction and CT analysis. The region of interest was set to a circular diameter of 8 mm in a coronal plane, to evaluate the new bone formation. The bone morphometric parameters analyzed were percentage of bone volume (BV/TV), trabecular bone pattern factor (Tb.Pf), trabecular thickness (Tb.Th), trabecular number (Tb.N), trabecular separation (Tb.Sp), bone surface/volume ratio (BS/BV), structure model index (SMI), and degree of anisotropy (DA).

2.13.2 Histology. The specimens were fixed with 10% formalin, dehydrated sequentially with 80–100% ethyl alcohol, and then embedded in Technovit 7200 (EXAKT, Germany) resin after being sequentially impregnated into dehydrated specimens. The specimens were solidified using a polymerization system (EXAKT, Germany); then, the blocks were attached to the acrylic slide, and the block was sectioned to a 200 μm-thick slice with an EXAKT cutter (EXAKT, Germany). Then, using an EXAKT grinding system machine (EXAKT, Germany), the slice was ground to a 30–50 μm thickness. The slices were stained with hematoxylin and eosin staining (H&E staining) and Masson trichrome staining, and the new bone formation was observed using a microscope.

2.14 Statistical analysis

All data were expressed as mean value ± standard deviation, and each experiment was performed in triplicate for three separate experiments. Data from the *in vitro* experiment were analyzed using a one-way analysis of variance (ANOVA) followed by Tukey's *post hoc* test. The statistical significance was $*p < 0.05$, $**p < 0.01$, and $***p < 0.001$. In addition, the data of the *in vivo* experiment were analyzed using a one-way ANOVA followed by analysis by SPSS 20 (IBM Corp., Armonk, NY: IBM Corp.). The statistical significance was $*p < 0.05$, $**p < 0.01$, $***p < 0.001$, and $****p < 0.0001$.

3. Results and discussion

In the present study, a new concept of a 3D indirect co-culture system was developed to mimic a bone tissue environment and to study the paracrine effect between ADSCs and osteoblasts. A 3D hydrogel scaffold was established with collagen type I, which is the main component of bone tissue.[4] In addition, osteoblasts, the main bone-active cells that form new bone tissue, were indirectly co-cultured with ADSCs. To confirm ADSC differentiation accurately, ADSCs and osteoblasts were separated by encapsulating the osteoblasts in alginate microbeads. This platform made it possible to collect only ADSCs and study the paracrine effect of osteoblasts in a 3D environment.

3.1 Fabrication and characterization of scaffolds

To generate a 3D indirect co-culture system, alginate microbeads were embedded in a collagen-based hydrogel scaffold (Fig. 1). The alginate microbeads were formed using electrostatic droplet extrusion, which is feasible, fast, and harmless for cell encapsulation. Before the cell encapsulation in alginate microbeads, we optimized fabrication conditions for uniform and size-controlled alginate microbeads. The size of the alginate microbeads decreased from 1200 to 450 μm as the electrical potential of electrostatic droplet extrusion increased (Fig. 2a and b).[26] In addition, the homogeneity of alginate microbeads increased as the electrical potential increased. Therefore, 450 μm alginate microbeads with the highest uniformity were selected for cell encapsulation. The alginate microbeads increased the 3D collagen hydrogel mechanical property when embedded in the collagen hydrogel (Fig. 2c).

3.2 *In vitro* characterization of encapsulated cells

Alginate microbeads embedded in a hydrogel complex were used to establish an indirect co-culture system by encapsulating two

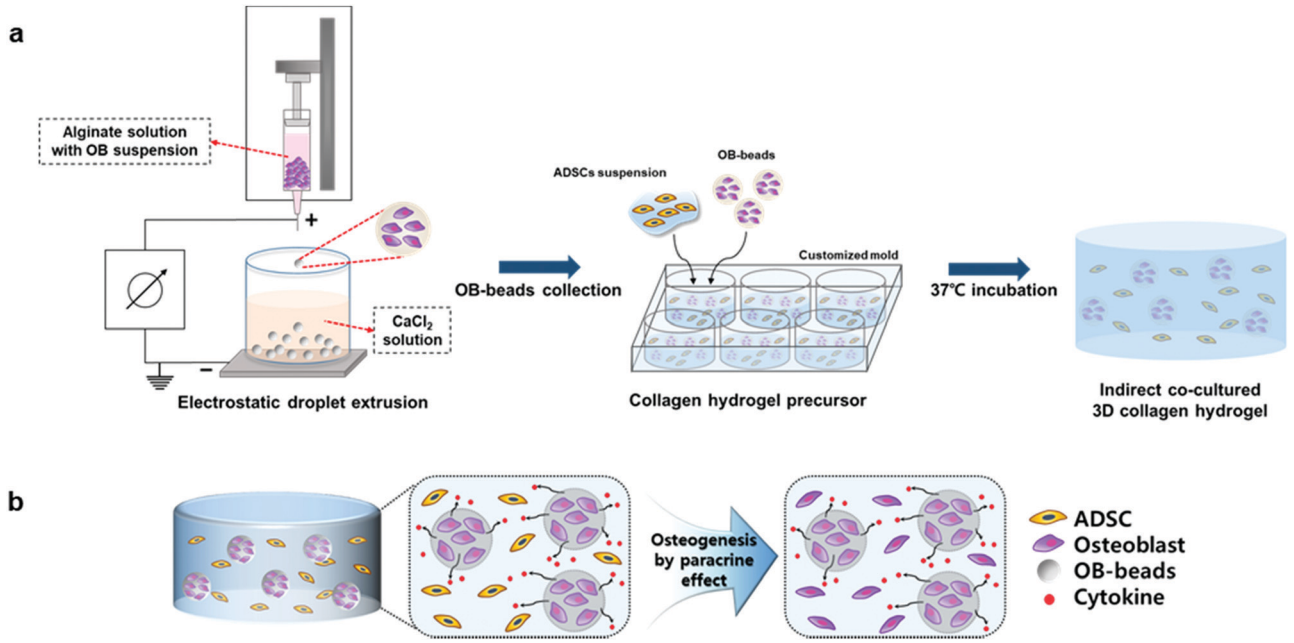

Fig. 1 Schematic illustration of a 3D indirect co-culture system based on the hydrogel. (a) The preparation procedure of an indirect co-cultured 3D collagen hydrogel. (b) ADSC differentiation to osteogenic lineage by the paracrine effect of osteoblasts encapsulated in microbeads.

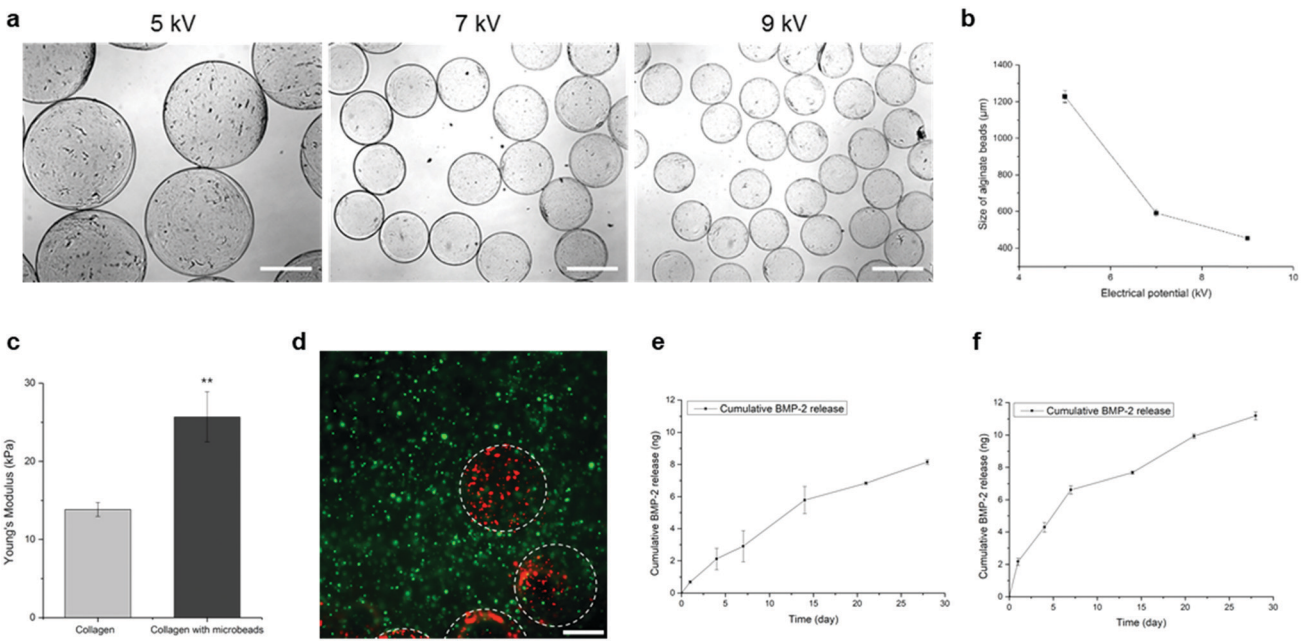

Fig. 2 Characterization of the scaffold. (a) Optical microscopy images of alginate microbeads fabricated by electrostatic droplet extrusion with different electrical potentials (kV) and (b) change of diameter. (c) Young's modulus of the collagen scaffold without or with alginate microbeads fabricated at 9 kV electrical potential. (d) Distribution of osteoblasts (red fluorescence) and ADSCs (green fluorescence) in the 3D indirect co-culture. Osteoblasts were encapsulated in alginate microbeads (OB-beads), and ADSCs were embedded in the collagen scaffold with OB-beads (scale bar, 500 μm). (e) Cumulative BMP-2 release profile from OB-beads and (f) BMP2-beads (** indicates $p < 0.01$, $n = 3$).

different cells in different regions. Osteoblasts were encapsulated in alginate microbeads (OB-beads), and ADSCs were encapsulated with OB-beads in the 3D collagen hydrogel. Two types of cells in the same batch were confirmed by fluorescence staining (Fig. 2d). Next, we examined the cumulative secreted amount of BMP-2 from OB beads and BMP2-beads, because BMP-2 primarily regulates the osteogenic differentiation of MSCs. To measure the amount of BMP-2 secreted from alginate microbeads, culture media and PBS were measured for OB-beads and BMP2-beads, respectively. A total of 8 ng of BMP-2 was released continuously

over 28 days from OB-beads (Fig. 2e). Moreover, BMP-2 was loaded in the alginate microbeads for the positive control group. Similar to the BMP-2 release behavior from OB-beads, a total amount of 11 ng was released in a sustained manner for 28 days from BMP2-beads (Fig. 2f). However, the result showed an initial burst release within seven days. The staining results confirmed that osteoblasts were encapsulated in the alginate microbeads and ADSCs were positioned in the peripheral region of OB-beads (Fig. 3a and b). For further long term culture, the cell viability in the indirect co-culture system was tested by live/dead staining and CCK-8 assay. The live/dead fluorescence staining result showed sustained living cells without significant cell death in the scaffold (Fig. 3c). Moreover, ADSCs proliferated well in the collagen scaffold, and are the main component of bone tissue, whereas osteoblasts encapsulated in alginate microbeads showed a round morphology without notable proliferation. In the CCK-8 assay, osteoblasts proliferated slightly, and the ADSC proliferation behavior increased in all groups (Fig. 3d). The result indicates that an indirect co-culture scaffold is suitable for cell viability and proliferation. It also shows that two different hydrogel regions impart various cell adhesion properties, because alginate is a hydrophilic biomaterial and has no ligands such as integrin receptors, $\alpha v\beta 3$, and $\alpha 5\beta 1$ to which mammalian cells attach.[27,28] Therefore, osteoblasts in alginate microbeads did not interact with any polymer that could reduce the proliferation rate, whereas MSCs showed a distinct proliferation in the collagen 3D microenvironment.

Previous studies have demonstrated that alginate microbeads supported the living cell viability and phenotypic stability of bovine articular chondrocytes.[29,30] Similarly, in our study alginate microbeads enabled long-term viability of osteoblasts and sustained release of BMP-2 secreted by osteoblasts. Additionally alginate microbeads provide different spaces for two types of cells in our system. Also, encapsulating osteoblasts using alginate microbeads regulates the proliferation and differentiation of osteoblasts by different alginate polymer compositions and gel mesh sizes.[31] In addition, compared with

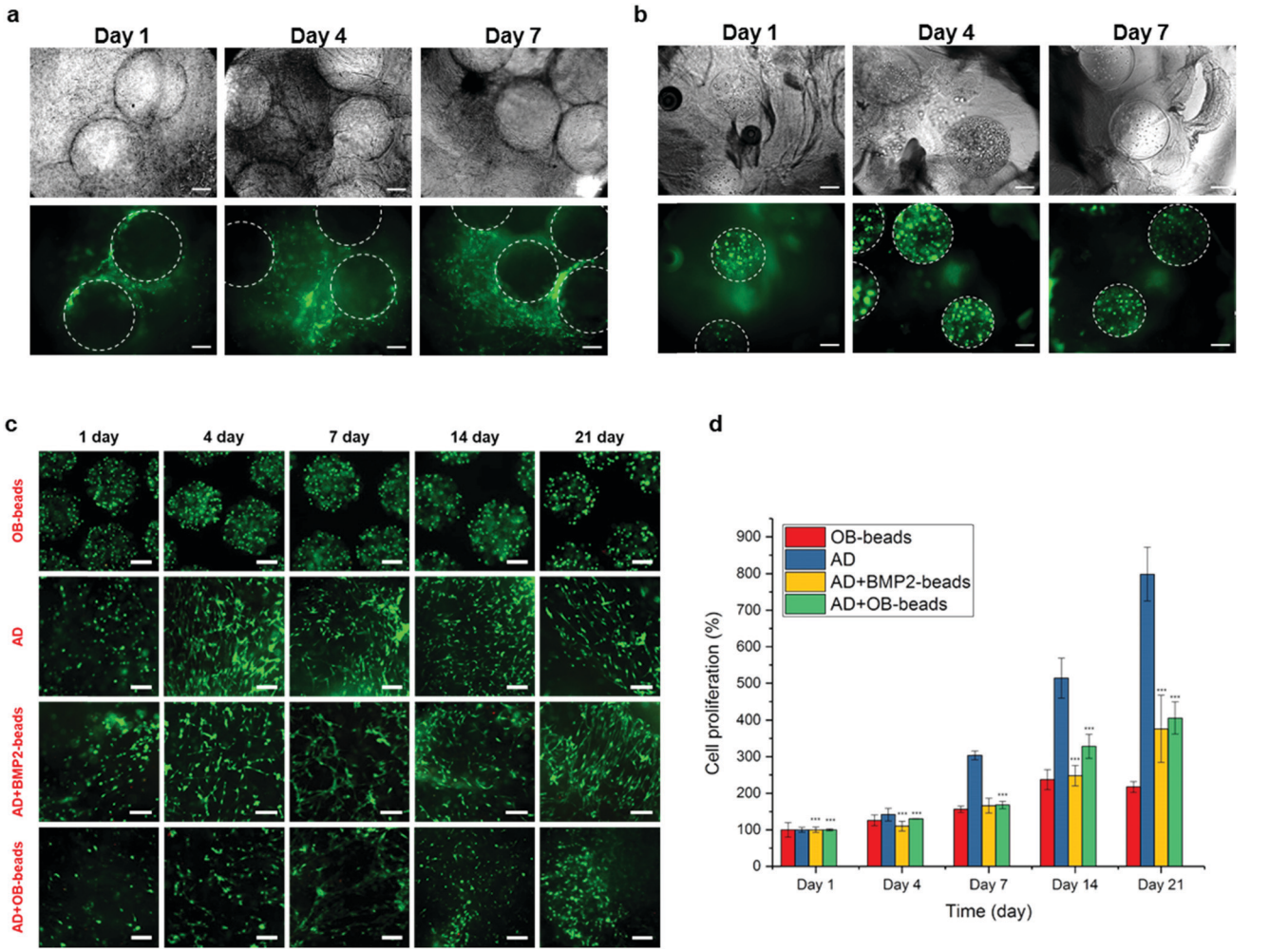

Fig. 3 Cell viability and position in an indirect co-culture system. (a) Green fluorescence Cell Tracker stained ADSCs and (b) osteoblasts placed in the outer and inner sides of alginate microbeads respectively maintained the position for culture period (scale bar, 200 μm). (c) Live and dead fluorescence staining of osteoblasts and ADSCs in OB-beads, AD, AD + BMP-2, and AD + OB-bead groups (scale bar, 200 μm). (d) Cell proliferation assay by CCK-8 analysis for 21 days (***, compared with the AD group within the same time point, $p < 0.001$, and $n = 3$).

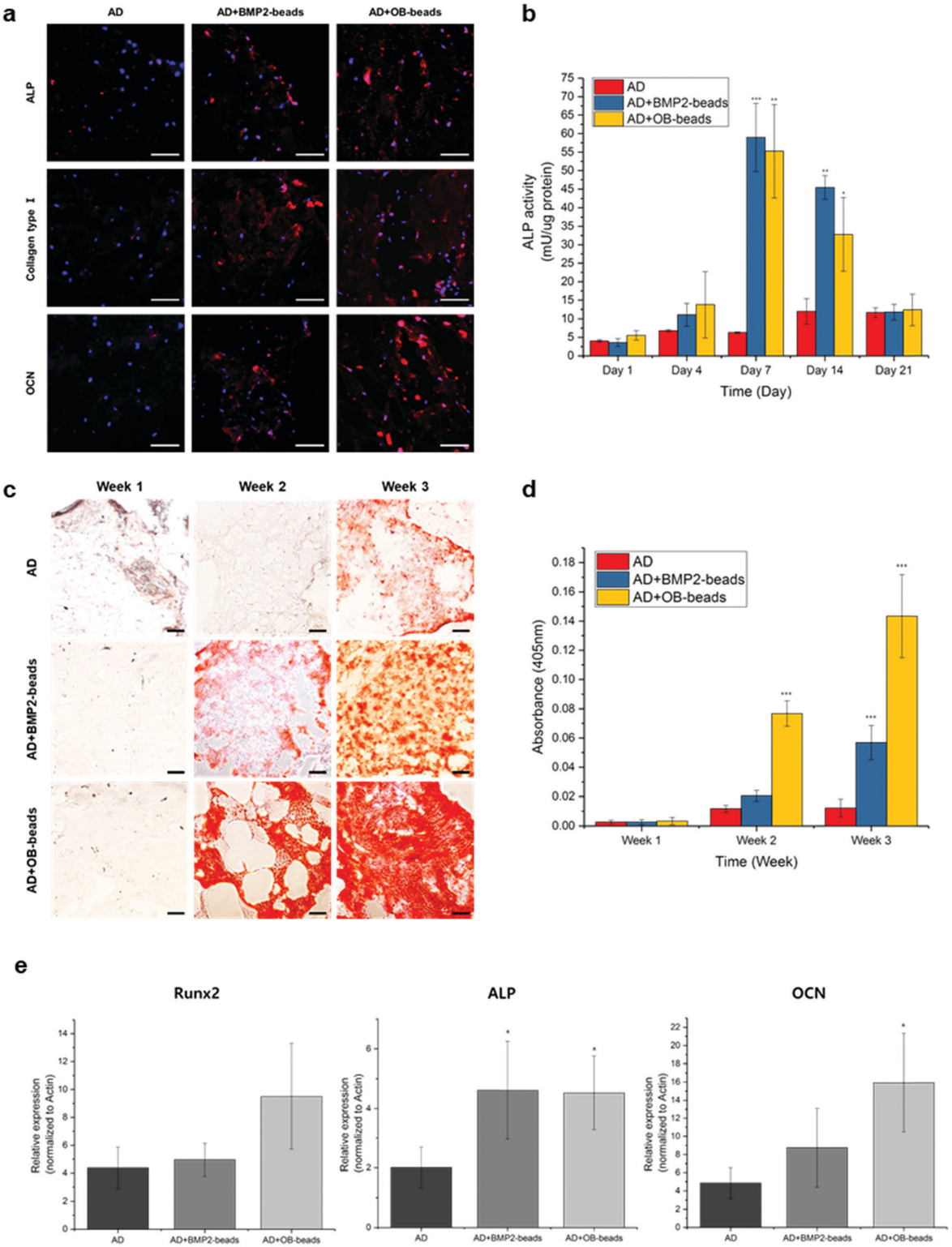

Fig. 4 *In vitro* osteogenic differentiation of ADSCs in the scaffold. (a) Immunofluorescence staining of Dapi (blue) and osteogenesis markers alkaline phosphatase (ALP), collagen type I, and osteocalcin (OCN) (red) at week 3 (scale bar, 100 μm). Dapi and osteogenic marker overlapped areas are shown in purple. (b) ALP activity for culture period. (c) Calcium deposition analysis by Alizarin red S staining of cryo-sectioned scaffolds (scale bar, 200 μm). (d) Quantification of Alizarin red S staining, which deposited in the bulk scaffolds. (e) mRNA expression levels for representative osteogenic markers Runx2, ALP, and OCN (*, **, ***, compared with the AD group within the same time point, * indicates $p < 0.05$, ** indicates $p < 0.01$, *** indicates $p < 0.001$, and $n = 3$).

the AD group, the proliferation of ADSCs was low in the AD + BMP2-bead and AD + OB-bead groups, indicating a differentiation capacity of ADSCs from day 7.

3.3 *In vitro* osteogenic differentiation of ADSCs

To investigate the osteogenic differentiation capacity of ADSCs in all scaffolds, immunofluorescence staining for osteogenic markers, ALP activity, and mRNA level expression were assessed. For ALP activity and mRNA level expression, only ADSCs were collected by collagen scaffold degradation and separating OB-beads for accurate analysis of MSC differentiation capacity. In the immunofluorescence staining results, the highest expression of ALP, collagen type I, and OCN occurred in the AD + OB-bead group on day 21 (Fig. 4a). Moreover, the ALP activities for AD + BMP2 and AD + OB groups increased significantly compared to the AD group, and peaked on day 7 but by day 21 the levels were not significantly different between the three groups (Fig. 4b) compared with the AD group. The highest expression of ALP activity occurred on day 7 and continuously decreased until day 21 except for the AD group. In the RT-qPCR results, the expression of ALP and OCN was significantly upregulated in the AD + OB-bead group on day 21 compared with the AD group (Fig. 4e). In particular, OCN, the last step marker of osteogenic differentiation, showed an expression level that correlated with the immunofluorescence result. Furthermore, the calcium deposition level in the scaffold was evaluated. As shown in Fig. 4c, Alizarin red S staining was increased for the culture period and the highest in the AD + OB-beads group. Finally, Alizarin red S was extracted from acetic acid to quantify calcium deposition in the scaffold (Fig. 4d). As shown in the staining images, the amount of Alizarin red S was higher in the AD + OB-bead group. Although the cumulative releasing profiles of BMP-2 from OB-beads and BMP-2 beads showed a similar tendency, the osteogenic differentiation effect was higher in the AD + OB-bead group. The expression of important osteogenic factors and the highest amount of calcium deposition in the AD + OB-bead group demonstrated that differentiation of ADSCs was most effective when ADSCs were co-cultured with osteoblasts.

Tsai *et al.* also demonstrated that osteoblasts induce osteogenic differentiation of MSCs by 2D direct co-culture.[32] Moreover, other researchers confirmed that osteoblasts initially stimulated MSC proliferation[33] and induced osteogenesis in the osteogenic niche.[34] Additionally, Huang *et al.* reported the importance of a 3D co-culture microenvironment to support active cell function compared with a 2D co-culture microenvironment.[35] According to previous studies and the present study, osteoblasts and bone-derived cells can function to induce osteogenic differentiation of stem cells. The differentiation of MSCs forward to osteogenic lineage is determined by complex regulatory factors in the microenvironment. In particular, BMP-2, 4, 6, and 7 have been regarded as important mediators for MSC differentiation for osteoblasts.[36] The intracellular effects of BMPs are regulated by an interaction with the cell surface BMP receptor (BMPR), and activation of BMPR type IB is crucial for osteogenic differentiation. When the BMPR is

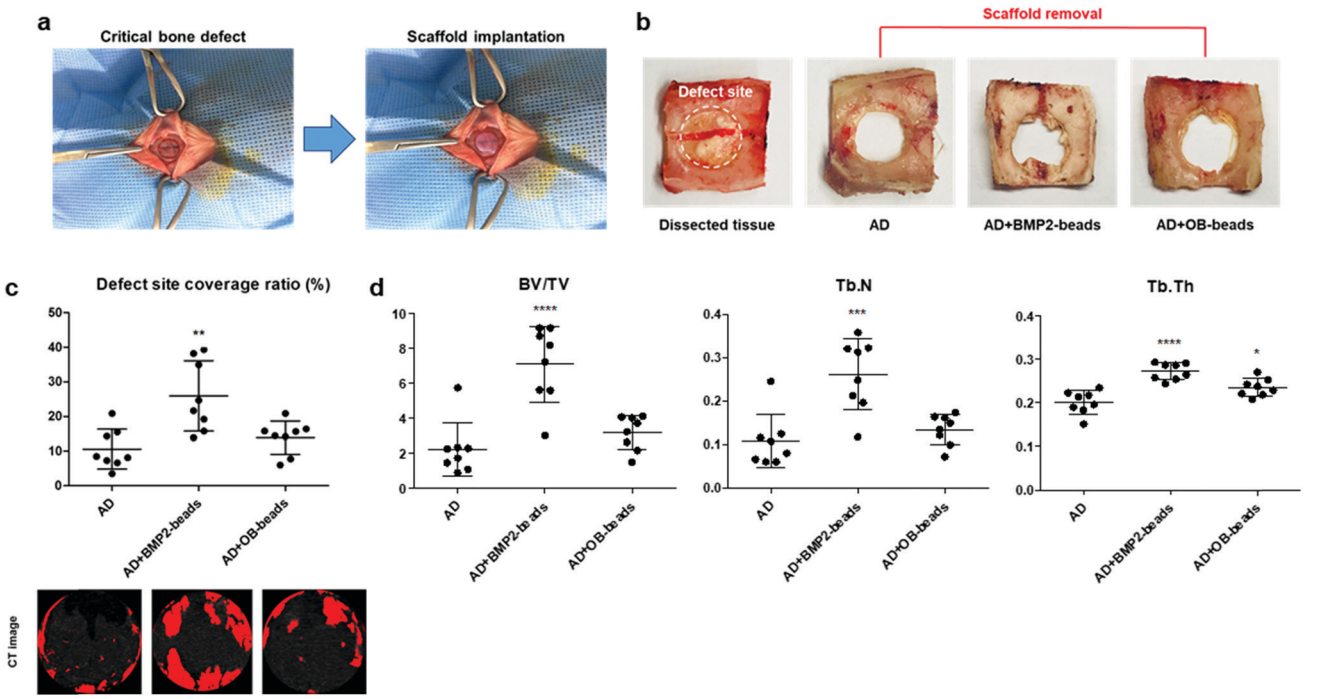

Fig. 5 *In vivo* bone tissue regeneration in the rat calvarial defect model. (a) 8 mm diameter of critical bone defect was developed and the three types of scaffolds were implanted. (b) The harvested bone defect site 6 weeks after transplantation. (c) Calculated defect site coverage ratio (%). (d) Calculated percent bone volume (BV/TV), trabecular number (Tb.N), and trabecular thickness (Tb.Th) (*, **, ***, ****, compared with the AD group, * indicates $p < 0.05$, ** indicates $p < 0.01$, *** indicates $p < 0.001$, and *** indicates $p < 0.0001$).

Table 1 CT parameters

Group (n)	BV/TV	BS/BY	Tb.Th	Tb.Sp	Tb.N	Tb.Pf	SMI	DA
	Average ± std							
AD (n = 8)	2.24 ± 1.52	21.33 ± 3.71	0.20 ± 0.03	1.35 ± 0.16	0.11 ± 0.06	15.00 ± 4.74	4.19 ± 1.05	2.63 ± 0.58
AD + BMP2-beads (n = 8)	7.09 ± 2.18*#	13.01 ± 1.55*#	0.27 ± 0.02*#	1.21 ± 0.18	0.26 ± 0.08*#	8.69 ± 4.26*	3.90 ± 1.72	2.36 ± 0.34
AD + OB-beads (n = 8)	3.19 ± 0.98	17.59 ± 3.01	0.23 ± 0.02*	1.36 ± 0.11	0.13 ± 0.04	10.61 ± 3.23	3.57 ± 0.77	2.28 ± 0.39
All P-value	$P < 0.001$	$P < 0.001$	$P < 0\ 001$	$P = 0.099$	$P < 0.001$	$P = 0.018$	$P = 0.623$	$P = 0.286$

*, compared with the Col/ADSC group, $p < 0.05$; #, compared with the Col/ADSC/E1 group, $p < 0.05$.

activated, Runx2 pathways are triggered, which enhances osterix formation, so that osteogenic differentiation is started. Although the BMP-2 release was similar in the OB-beads and BMP2-beads in the present study, the high osteogenic effect in OB-beads can be regarded as the effect of various cytokine complexes, including the TGF-β family, fibroblast growth factor-2 (FGF-2), and insulin-like growth factor[37] released by osteoblasts.

In terms of the importance of the 3D biomimetic micro-environment for cell behavior and tissue regeneration,[38] a co-culture system has also been developed in a 3D platform with various cell types.[39] However, because of direct contact between stem cells and organotypic cells in 3D direct co-culture systems, it is unclear to distinguish where stem cells differentiated into organotypic cells or not. Therefore, our indirect co-culture platform can resolve this challenge as clear isolation by spatial separation of MSCs and osteoblasts. *In vitro* osteogenic differentiation investigation proved that an indirect co-culture system is beneficial for osteogenesis of MSCs and also the easy separation of MSCs and osteoblasts for precise evaluation.

3.4 *In vivo* osteogenic effect of ADSCs in a calvarial defect model

3.4.1 Micro-CT results. During the experiment, no animals experienced inflammation, infection, and death. The calvarial defect model was used to confirm the osteogenic effect of ADSCs in 3D scaffolds. After surgery, scaffolds were implanted successfully at the defect site (Fig. 5a). After six weeks, the defect site tissues were harvested, and it was observed that there was bone tissue reconstruction at the edge site in the AD + BMP2-bead and AD + OB-bead groups (Fig. 5b). In addition, the coverage ratio of the defect site was higher in the AD + BMP2-bead (coverage ratio: 25.9 ± 10.17) and AD + OB-bead (coverage ratio: 13.84 ± 4.79, p = 0.001) groups than in the AD group (coverage ratio: 10.56 ± 5.73, p = 0.001) (Fig. 5c and Table 1). Specifically, in the CT images, new bone formation from the margin to the center of the defect was observed in the AD + BMP2-bead and AD + OB-bead groups (Fig. 5c). The calculated parameters, including BV/TV, Tb.N, and Tb.Th, showed high values in the AD + BMP-2 bead group and a slight increase in the AD + OB-bead group (Fig. 5d).

3.4.2 Histological result. New bone tissue formation was observed in all groups in the H&E staining results. The newly formed bone thickness and length were higher in the AD + BMP2-bead and AD + OB-bead groups, whereas the AD group showed minimal new bone formation at the defect site, limited to the edge of the host bone (Fig. 6a). Furthermore, Masson's trichrome staining indicated that collagen tissue was significantly formed in the AD + BMP2-bead and AD + OB-bead groups; however, there was a lack of collagen tissue formation in the AD group (Fig. 6b).

In the study of osteogenic differentiation of MSCs *in vivo*, new bone tissue formation was observed in the AD + BMP2-bead and

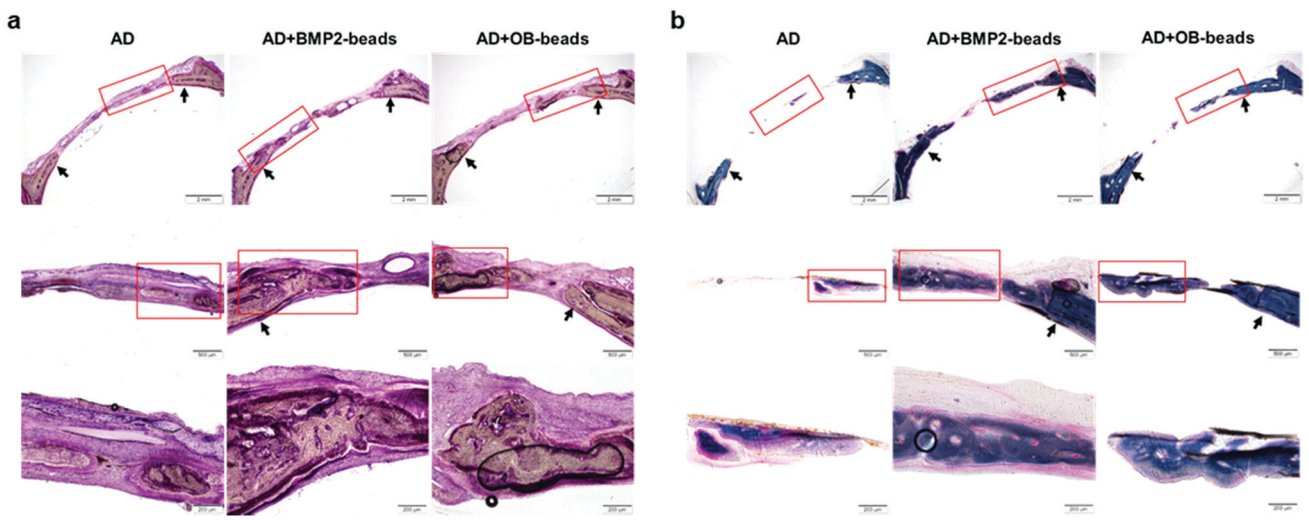

Fig. 6 Histological result of the calvarial defect site. (a) Hematoxylin and eosin (H&E) staining and (b) Masson's trichrome staining of bone defect tissue (black arrow, host bone tissue; scale bar of images from top to bottom, 2 mm, 500 μm, and 200 μm).

AD + OB-bead groups six weeks after scaffold implantation in the calvarial defect model (Fig. 5). The micro-CT images and histology results imply that osteogenic differentiation of MSCs in the scaffold was accomplished when co-cultured with OB-beads and BMP2-beads. However, the bone formation effect of MSCs in AD + OB-beads was lower than that in the *in vitro* results. This result may be immune rejection due to the transplantation of mouse-derived osteoblasts and human-derived MSCs in the rat an *in vivo* environment. Other studies have found that xenotransplantation into a bone defect model causes immunocompetence and hinders bone regeneration.[40,41] This result suggests that it is important to solve the immunogenicity of the implant to maximize tissue regeneration effects. In addition, the samples were harvested six weeks after implantation, which could indicate an insufficient culture period for MSC osteogenesis without any exogenous factors. A further study is necessary with co-culture between allogeneic cells and long-term *in vivo* experiments to investigate fully formed bone tissue in the co-culture system with the absence of any artificial factors. However, as a promising therapeutic tool, the indirect co-culture system proved to be more effective for bone regeneration compared with an ADSC only culture system, demonstrating that bone tissue regeneration can be enhanced by mimicking a bone tissue microenvironment without exogenous factors, such as BMP-2. In addition, this system can be an effective tool for studying the paracrine effect between different types of cells in a 3D microenvironment.

4. Conclusions

In this study, a novel indirect 3D co-culture system based on a hydrogel scaffold was developed. Separate spaces for ADSCs and osteoblasts were designed for accurate analysis of stem cell differentiation function in a 3D microenvironment. In this system, osteoblasts successfully induced osteogenic differentiation of ADSCs without any exogenous factors, which is a positive achievement in stem cell therapy for bone regeneration. Ultimately, an osteogenesis effect was verified in the indirect co-culture group compared with the ADSC monoculture group in a rat calvarial defect model. This new concept of an indirect co-culture system could provide a tool for cell communication study and an *in vitro* tissue platform for tissue regeneration.

Author contributions

H. K. and Y.-M. K. conceived the idea and performed the *in vitro* experiments which were supervised by K. L. and W.-G. K. S. H. H. and Y.-Z. J. performed *in vivo* experiments which were supervised by J. H. L. K.-M. L. supported performing the experiments and data analysis. H. K., Y.-M. K., and S. H. H. wrote the whole manuscript, which was edited by W.-G. K., J. H. L., and K. L.

Conflicts of interest

There are no conflicts to declare.

Acknowledgements

This work was supported by the Collaborative Research Program of SNU Boramae Medical Center and Basic Medical Science from Seoul National University College of Medicine (800-20170005; J. H. Lee). This work was also supported by the National Research Foundation of Korea (NRF) funded by the Ministry of Science, ICT & Future Planning (2016M3A9B4919711; K. Lee, and 2017M3A7B4041798 and 2018M3A9E2024583; W.-G. Koh). Lastly, this work was supported by NRF (National Research Foundation of Korea) Grant funded by the Korean Government (NRF-2017-Global PhD Fellowship Program; H. Kim).

References

1 C. Zheng, J. Chen, S. Liu and Y. Jin, *Int. J. Oral Sci.*, 2019, **11**, 23.
2 T. Gong, J. Xie, J. Liao, T. Zhang, S. Lin and Y. Lin, *Bone Res.*, 2015, **3**, 15029.
3 G. Fernandes and S. Yang, *Bone Res.*, 2016, **4**, 16036.
4 J. Henkel, M. A. Woodruff, D. R. Epari, R. Steck, V. Glatt, I. C. Dickinson, P. F. Choong, M. A. Schuetz and D. W. Hutmacher, *Bone Res.*, 2013, **1**, 216–248.
5 S. Asgary, *Iran. Endod. J.*, 2009, **4**, 117–121.
6 S. Bose and M. Roy, *Trends Biotechnol.*, 2012, **30**, 546–554.
7 M. E. Aichelmann-Reidy and R. A. Yukna, Bone replacement grafts. The bone substitutes, *Dent. Clin. North Am.*, 1998, **42**, 491–503.
8 M. A. Reynolds, M. E. Aichelmann-Reidy and G. L. Branch-Mays, *Dent. Clin. North Am.*, 2010, **54**, 55–71.
9 Y. Yamada, K. Ito, S. Nakamura, M. Ueda and T. Nagasaka, *Cell Transplant.*, 2011, **20**, 1003–1013.
10 G. G. Walmsley, R. C. Ransom, E. R. Zielins, T. Leavitt, J. S. Flacco, M. S. Hu, A. S. Lee, M. T. Longaker and D. C. Wan, *Stem Cell Rev. Rep.*, 2016, **12**, 524–529.
11 J. L. Crane and X. Cao, *J. Clin. Invest.*, 2014, **124**, 466–472.
12 O. D. de Lageneste, A. Julien, R. Abou-Khalil, G. Frangi, C. Carvalho, N. Cagnard, C. Cordier, S. J. Conway and C. Colnot, *Nat. Commun.*, 2018, **9**, 773.
13 L. M. Calvi, G. B. Adams, K. W. Weibrecht, J. M. Weber, D. P. Olson, M. C. Knight, R. P. Martin, E. Schipani, P. Divieti, F. R. Bringhurst, L. A. Milner, H. M. Kronenberg and D. T. Scadden, *Nature*, 2003, **425**, 841–846.
14 Y. Han, X. You, W. Xing, Z. Zhang and W. Zou, *Bone Res.*, 2018, **6**, 16.
15 U. H. Weidle, F. Birzele, G. Kollmorgen and R. Ruger, *Cancer Genomics Proteomics*, 2016, **13**, 1–12.
16 H. Qiao and T. T. Tang, *Bone Res.*, 2018, **6**, 16.
17 H. Kim, J. H. Lee and H. Suh, *Yonsei Med. J.*, 2003, **44**, 187–197.
18 Y. Wang, V. Volloch, M. A. Pindrus, D. J. Blasioli, J. Chen and D. L. Kaplan, *J. Tissue Eng. Regener. Med.*, 2007, **1**, 39–50.
19 M. Glueck, O. Gardner, E. Czekanska, M. Alini, M. J. Stoddart, G. M. Salzmann and H. Schmal, *BioRes. Open Access*, 2015, **4**, 121–130.

20 F. Bohrnsen and H. Schliephake, *Int. J. Oral Sci.*, 2016, **8**, 223–230.
21 Y. L. Wang, F. Jiang, Y. Liang, M. Shen and N. Chen, *Stem Cells Int.*, 2016, **2016**, 4851081.
22 M. E. Wechsler, R. E. Stephenson, A. C. Murphy, H. F. Oldenkamp, A. Singh and N. A. Peppas, *Biomed. Microdevices*, 2019, **21**, 31.
23 N. M. B. Smeets and T. Hoare, *J. Polym. Sci., Polym. Chem. Ed.*, 2013, **51**, 3027–3043.
24 K. Wang, S. Lin, K. C. Nune and R. D. Misra, *J. Biomater. Sci., Polym. Ed.*, 2016, **27**, 441–453.
25 D. Thomas, G. Marsico, I. L. Mohd Isa, A. Thirumaran, X. Chen, B. Lukasz, G. Fontana, B. Rodriguez, M. Marchetti-Deschmann, T. O'Brien and A. Pandit, *Proc. Natl. Acad. Sci. U. S. A.*, 2020, **117**, 19033–19044.
26 T. I. Klokk and J. E. Melvik, *J. Microencapsulation*, 2002, **19**, 415–424.
27 K. Y. Lee and D. J. Mooney, *Prog. Polym. Sci.*, 2012, **37**, 106–126.
28 J. A. Rowley, G. Madlambayan and D. J. Mooney, *Biomaterials*, 1999, **20**, 45–53.
29 W. Zhang and X. He, *J. Biomech. Eng.*, 2009, **131**, 074515.
30 H. J. Hauselmann, R. J. Fernandes, S. S. Mok, T. M. Schmid, J. A. Block, M. B. Aydelotte, K. E. Kuettner and E. J. Thonar, *J. Cell Sci.*, 1994, **107**, 17–27.
31 B. H. Lee, B. Li and S. A. Guelcher, *Acta Biomater.*, 2012, **8**, 1693–1702.
32 M. T. Tsai, D. J. Lin, S. Huang, H. T. Lin and W. Chang, *Int. Orthop.*, 2012, **36**, 199–205.
33 E. Birmingham, G. L. Niebur, P. E. McHugh, G. Shaw, F. P. Barry and L. M. McNamara, *Eur. Cells Mater.*, 2012, **23**, 13–27.
34 Z. F. Lu, S. I. Roohani-Esfahani, P. C. L. Kwok and H. Zreiqat, *Tissue Eng., Part A*, 2011, **17**, 1651–1661.
35 X. Huang, B. Zhu, X. Wang, R. Xiao and C. Wang, *Int. J. Mol. Med.*, 2016, **38**, 1141–1151.
36 S. Muruganandan, A. A. Roman and C. J. Sinal, *Cell. Mol. Life Sci.*, 2009, **66**, 236–253.
37 W. Huang, S. Yang, J. Shao and Y. P. Li, *Front. Biosci.*, 2007, **12**, 3068–3092.
38 H. Kim, C. Bae, Y. M. Kook, W. G. Koh, K. Lee and M. H. Park, *Stem Cell Res. Ther.*, 2019, **10**, 51.
39 Y. M. Kook, Y. Jeong, K. Lee and W. G. Koh, *J. Tissue Eng.*, 2017, **8**, 2041731417724640.
40 K. Takeshita, S. Motoike, M. Kajiya, N. Komatsu, M. Takewaki, K. Ouhara, T. Iwata, K. Takeda, N. Mizuno, T. Fujita and H. Kurihara, *Stem Cell Res. Ther.*, 2017, **8**, 101.
41 H. Tang, B. Wu, X. Qin, L. Zhang, J. Kretlow and Z. F. Xu, *J. Cardiothorac. Surg.*, 2013, **8**, 133.